

Fast Point Transformer

Chunghyun Park

Yoonwoo Jeong

Minsu Cho

Jaesik Park

POSTECH CSE & GSAI

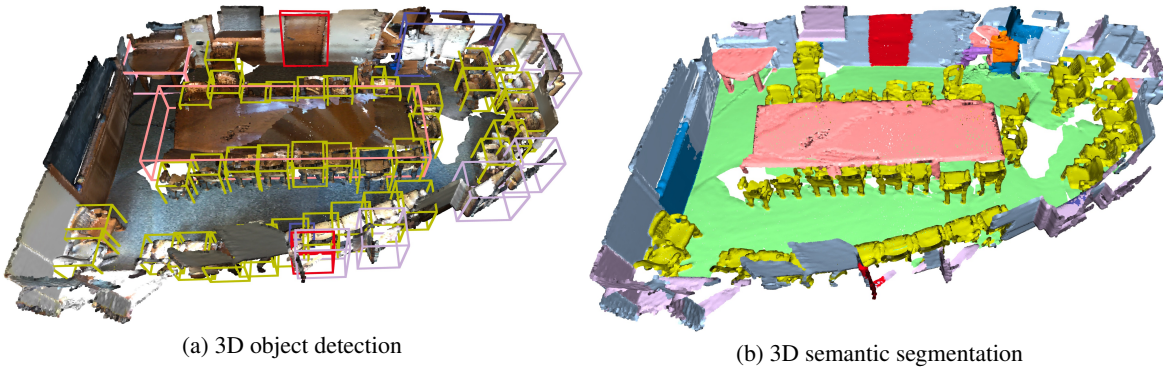


Figure 1. **Fast Point Transformer** can process large-scale scenes using a local self-attention mechanism. Unlike Point Transformer [46], our approach can infer the scene at one shot without searching point-wise neighbors. The average inference time of our network is 0.13 seconds per scene, resulting in 136 times faster than Point Transformer.

Abstract

The recent success of neural networks enables a better interpretation of 3D point clouds, but processing a large-scale 3D scene remains a challenging problem. Most current approaches divide a large-scale scene into small regions and combine the local predictions together. However, this scheme inevitably involves additional stages for pre- and post-processing and may also degrade the final output due to predictions in a local perspective. This paper introduces **Fast Point Transformer** that consists of a new lightweight self-attention layer. Our approach encodes continuous 3D coordinates, and the voxel hashing-based architecture boosts computational efficiency. The proposed method is demonstrated with 3D semantic segmentation and 3D detection. The accuracy of our approach is competitive to the best voxel-based method, and our network achieves 136 times faster inference time than the state-of-the-art, Point Transformer, with a reasonable accuracy trade-off.

1. Introduction

3D scene understanding is a fundamental task due to its importance to various fields, such as robotics, intelligent agents, and AR/VR. Recent approaches [5, 9, 20, 23, 24, 32, 34] utilize the deep learning frameworks, but processing a

large-scale 3D scene as a whole remains a challenging problem because it involves extensive computation and memory budgets. As an alternative, some methods crop 3D scenes and stitch predictions [17, 23, 24, 32, 33, 38], or others approximate point coordinates for efficiency [5, 9, 21, 47]. Such techniques, however, typically lead to a substantial increase of inference time and/or degrade the final output due to the local or approximate predictions. Achieving both fast inference time and high accuracy is thus one of the primary challenges in the 3D scene understanding tasks.

The pioneering 3D understanding approaches, PointNet [23] and PointNet++ [24] process point clouds with multi-layer perceptrons (MLPs), which preserve permutation-invariance of the point clouds. Such *point-based methods* introduce impressive results [20, 34] recently, and Point Transformer [46] shows superior accuracy based on the local self-attention mechanism. However, it involves manual grouping of point clouds using k nearest neighbor search. In addition, applying scene-level inference with the point-based methods requires cropping scenes and stitching the predictions. *Voxel-based methods* [5, 9, 21, 47] are alternatives for a large-scale 3D scene understanding due to their effectiveness of the network design. However, they may lose fine geometric patterns due to quantization artifacts. *Hybrid methods* [19, 31, 32] reduce the quantization artifacts by utilizing *both* point-level and voxel-level features. However, approaches in this category require additional memory space

to cache both features.

We propose Fast Point Transformer, which effectively encodes continuous positional information of large-scale point clouds. Our approach leverages local self-attention [26, 35] of point clouds with voxel hashing architecture. To achieve higher accuracy, we present centroid-aware voxelization and devoxelization techniques that preserve the embedding of continuous coordinates. The proposed approach reduces quantization artifacts, and it allows the coherency of dense predictions regardless of rigid transformations. We also introduce a reformulation of the standard local self-attention equation to reduce space complexity further. The proposed local self-attention module can replace the convolutional layers for 3D scene understanding. Based on this, we introduce a local self-attention based U-shaped network, which naturally builds a feature hierarchy without manual grouping of point clouds. As a result, Fast Point Transformer collects rich geometric representations and exhibits a fast inference time even for large-scale scenes.

We conduct experiments using two datasets of large-scale scenes: S3DIS [1] and ScanNet [6]. Our method shows competitive accuracy in the semantic segmentation task on various voxel hashing configurations. We also apply the Fast Point Transformer network as a backbone of VoteNet [22] to show the applicability in the 3D object detection task. We use ScanNet [6] dataset for the 3D detection, and our model shows better accuracy (mAP) than other baselines that use point- or voxel-based network backbones. Besides, we introduce a novel consistency score metric, named CScore, and demonstrate that our model outputs more coherent predictions under rigid transformations.

In summary, our contributions are as follows:

1. We propose a novel local self-attention-based network, called Fast Point Transformer that can handle large-scale 3D scenes quickly.
2. We introduce a lightweight local self-attention module to reduce space complexity.
3. The proposed method effectively learns continuous positional information of 3D point clouds. We demonstrate that our model produces much more coherent predictions than the previous voxel-based approach using the proposed evaluation metric.
4. Our model shows fast inference time using voxel hashing-based architecture. Our network shows 136 times faster inference time than Point Transformer with a reasonable accuracy trade-off.

2. Related Work

In this section, we review point-based, voxel-based, and hybrid methods for 3D scene understanding and then revisit the attention-based models.

Point-based methods. PointNet [23] introduces a multi-layer perceptrons (MLP) based approach for understanding 3D scenes. PointNet++ [24] advances the PointNet [23] by adding hierarchical sampling strategies. Recent studies attempt to apply convolution on point clouds since the heuristic local sampling and grouping mechanisms used in PointNet++ [24] can be represented by the convolution. However, applying convolution on point clouds is challenging since 3D points are sparse and unordered. KPConv [34] mimics convolution using kernel points defined in the continuous space. They construct a k -d tree to perform point-wise convolution on the query points within a certain radius at the inference stage in exchange for inefficiency at the data preprocessing stage. Mao et al. [20] adopt discretized convolution kernels instead of continuous kernels for efficiency and perform convolution on every point in a point cloud, which poses a bottleneck when processing large-scale 3D scene point clouds. More recently, Guo et al. [10] and Zhao et al. [46] utilize local self-attention operations to learn richer feature representations than the fixed kernel-base methods [20, 34]. In fact, most point-based methods [10, 20, 23, 24, 34, 46] adopt expensive operations, such as k nearest neighbor search or k -d tree construction, resulting in heavy computational overhead when processing large-scale 3D scenes.

Voxel-based methods. Sparse convolution [5, 9] constructs fully convolutional neural networks using discrete sparse tensors, enabling fast processing of voxel data. The sparse convolution performs convolution to all valid neighbor voxels that are efficiently found using a hash table with constant time complexity, *i.e.*, $\mathcal{O}(1)$. Mao et al. [21] propose a voxel-based transformer architecture that adopts both local and dilated attention to enlarge receptive fields of the model. Despite the effectiveness of voxel-based work on large-scale point clouds, they often fail to capture fine patterns of point clouds due to the quantization artifacts produced during voxelization. In other words, the features extracted by voxel-based methods are inconsistent regarding the voxel size [43].

Hybrid methods. Another approach to handle point clouds is to extract both point- and voxel-level features. Recent work [19, 31, 41, 42] attaches point-based layers, *e.g.* *mini-PointNet*, on top of the voxel-based methods to relieve the quantization artifacts produced during voxelization. They take advantage of fast neighbor search of voxel-based methods and high capability of capturing fine-geometries of point-based methods. However, the hybrid methods suffer from larger computation and memory budgets since these approaches store both point- and voxel-level features.

Attention-based Networks. Discussions regarding attention operation have dominated research in recent years in Natural Language Processing [7, 25, 36]. Moreover, recent vision work [2, 8, 11, 40] has attempted to exploit the advantages of attention-based models. Prior research generally confirms that global self-attention is infeasible to

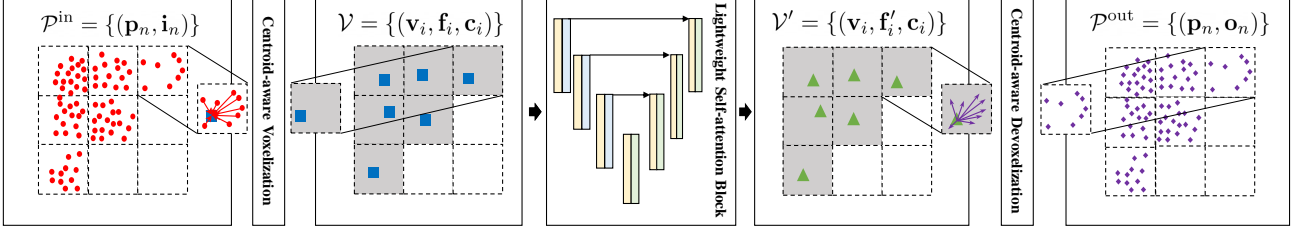


Figure 2. **Overall architecture.** We illustrate the overall architecture of the proposed Fast Point Transformer. The red points are input points and their features, and the purple points are output points and their features. The colored squares are non-empty voxels produced by voxelization. The blue and green points are centroids of non-empty voxels with their features.

be adopted in 3D vision tasks due to its costly operations. Thus, recent work [10, 21, 46] widely utilizes local self-attention [2, 26, 35] to process 3D point clouds. Guo et al. [10] and Zhao et al. [46] handle irregularity of point clouds with k nearest neighbor search, resulting in a remarkable performance gain.

3. Fast Point Transformer

3.1. Overview

Fast Point Transformer processes the point cloud through three steps: (Step 1) Centroid-aware voxelization, (Step 2) Lightweight self-attention, and (Step 3) Centroid-aware devoxelization. Figure 2 shows the overall architecture.

(Step 1) Let $\mathcal{P}^{\text{in}} = \{(\mathbf{p}_n, \mathbf{i}_n)\}_{n=1}^N$ be an input point cloud, where \mathbf{p}_n is the n -th point coordinate and \mathbf{i}_n is any raw input feature of \mathbf{p}_n , e.g., color of point clouds. For the computational efficiency, our approach voxelizes \mathcal{P}^{in} into $\mathcal{V} = \{(\mathbf{v}_i, \mathbf{f}_i, \mathbf{c}_i)\}_{i=1}^I$, a set of tuples. Each tuple contains i -th voxel coordinate \mathbf{v}_i , voxel feature \mathbf{f}_i , and voxel centroid coordinate \mathbf{c}_i . We introduce a centroid-aware voxelization process that utilizes learnable positional embedding \mathbf{e}_n between n -th point and its voxel centroid to minimize the loss from the quantization procedure.

(Step 2) Lightweight Self-Attention (LSA) block takes $\mathcal{V} = \{(\mathbf{v}_i, \mathbf{f}_i, \mathbf{c}_i)\}$ and updates the feature \mathbf{f}_i to the output feature \mathbf{f}'_i using local self-attention. In this procedure, querying neighbor voxels can be done with voxel hashing having $\mathcal{O}(N)$ complexity.

(Step 3) The output voxels $\mathcal{V}' = \{(\mathbf{v}_i, \mathbf{f}'_i, \mathbf{c}_i)\}$ from the attention block are devoxelized into the output point cloud $\mathcal{P}^{\text{out}} = \{(\mathbf{p}_n, \mathbf{o}_n)\}_{n=1}^N$, where \mathbf{o}_n is the output point feature. We propose to use learnable positional embedding \mathbf{e}_n to properly assign voxel-wise features to the continuous 3D points.

3.2. Centroid-aware Voxel&Devoxelization

Centroid-aware Voxelization. Let us consider an input point cloud $\mathcal{P}^{\text{in}} = \{(\mathbf{p}_n, \mathbf{i}_n)\}$. We voxelize input points for fast and scalable querying. The output voxels are denoted by $\mathcal{V} = \{(\mathbf{v}_i, \mathbf{f}_i, \mathbf{c}_i)\}$. We introduce a novel *centroid-to-point* positional encoding $\mathbf{e}_n \in \mathbb{R}^{D_{\text{enc}}}$ to mitigate the geometric

information loss during voxelization. With an encoding layer $\delta_{\text{enc}} : \mathbb{R}^3 \mapsto \mathbb{R}^{D_{\text{enc}}}$, the *centroid-to-point* positional encoding \mathbf{e}_n is defined as follows:

$$\mathbf{e}_n = \delta_{\text{enc}}(\mathbf{p}_n - \mathbf{c}_{i=\mu(n)}), \quad (1)$$

where centroid \mathbf{c}_i is $\mathbf{c}_i = \frac{1}{|\mathcal{M}(i)|} \sum_{n \in \mathcal{M}(i)} \mathbf{p}_n$, $\mathcal{M}(i)$ is a set of point indices within the i -th voxel, and $\mu : \mathbb{N} \mapsto \mathbb{N}$ is an index mapping from a point index n to its corresponding voxel index i . We define the output voxel feature $\mathbf{f}_i \in \mathbb{R}^{D_{\text{in}}+D_{\text{enc}}}$ with the input point feature $\mathbf{i}_n \in \mathbb{R}^{D_{\text{in}}}$ and the encoding \mathbf{e}_n as follows:

$$\mathbf{f}_i = \Omega_{n \in \mathcal{M}(i)}(\mathbf{i}_n \oplus \mathbf{e}_n), \quad (2)$$

where \oplus denotes vector concatenation and Ω is a permutation-invariant operator, e.g., average(\cdot).

We state that some voxel-based methods [29, 30, 42] introduce barycentric interpolation to embed \mathbf{f}_i into *regular* grids \mathbf{v}_i for voxelization. The proposed centroid-aware voxelization is different from those methods in that it encodes the *centroid-to-point* position into \mathbf{f}_i at *continuous* centroid coordinate \mathbf{c}_i . The proposed centroid-aware voxelization is also different from other class of voxel-based methods [5, 9, 21] that apply average- or max-pool voxel features without using intra-voxel coordinates of points.

Centroid-aware Devoxelization. Since the *centroid-to-point* positional encoding \mathbf{e}_n has a useful information about the relative position between \mathbf{p}_n and \mathbf{c}_i , we can propose a centroid-aware devoxelization process. Given an output voxels $\mathcal{V}' = \{(\mathbf{v}_i, \mathbf{f}'_i, \mathbf{c}_i)\}$ with the output voxel feature $\mathbf{f}'_i \in \mathbb{R}^{D_{\text{out}}}$, the proposed centroid-aware devoxelization process is formulated as follows:

$$\mathbf{o}_n = \text{MLP}(\mathbf{f}'_{i=\mu(n)} \oplus \mathbf{e}_n), \quad (3)$$

where $\mathbf{o}_n \in \mathbb{R}^{D_{\text{out}}}$ is the n -th output point feature of the output point cloud $\mathcal{P}^{\text{out}} = \{(\mathbf{p}_n, \mathbf{o}_n)\}$ and $\text{MLP}(\cdot) : \mathbb{R}^{D_{\text{out}}+D_{\text{enc}}} \mapsto \mathbb{R}^{D_{\text{out}}}$ denotes a multilayer perceptron.

3.3. Lightweight Self-Attention

Local self-attention on centroids. Once an input point cloud $\mathcal{P}^{\text{in}} = \{(\mathbf{p}_n, \mathbf{i}_n)\}$ is transformed into a set of voxels $\mathcal{V} = \{(\mathbf{v}_i, \mathbf{f}_i, \mathbf{c}_i)\}$, we can apply local self-attention

mechanism [27, 44, 48] with \mathcal{V} . In this procedure, we can query neighboring voxels quickly via voxel-hashing, which requires $\mathcal{O}(N)$ complexity. Note that point-based methods [38, 46] need to build neighbors using k nearest neighbor search having the complexity of $\mathcal{O}(N \log N)$, which become burdensome for processing large-scale point clouds. Given local neighbor indices of \mathbf{c}_i denoted by $\mathcal{N}(i)$, local self-attention on \mathbf{c}_i can be formulated as follows:

$$\mathbf{f}'_i = \sum_{j \in \mathcal{N}(i)} a(\mathbf{f}_i, \delta(\mathbf{c}_i, \mathbf{c}_j)) \psi(\mathbf{f}_j), \quad (4)$$

where \mathbf{f}'_i is output feature, $a(\mathbf{f}_i, \delta(\mathbf{c}_i, \mathbf{c}_j))$ is a function of attention weights using positional encoding $\delta(\mathbf{c}_i, \mathbf{c}_j)$ and ψ is the value projection layer.

Although the voxel hashing enables an fast neighbor search with time complexity of $\mathcal{O}(1)$ for a single query, designing an memory-efficient form of continuous positional encoding $\delta(\mathbf{c}_i, \mathbf{c}_j)$ still remains challenging problem. Specifically, Point Transformer [46] uses $\text{MLP}(\mathbf{c}_i - \mathbf{c}_j)$ for implementing $\delta(\mathbf{c}_i, \mathbf{c}_j) \in \mathbb{R}^D$, but it requires $\mathcal{O}(NKD)$ space complexity, where K is the cardinality of neighboring voxels. This is because there can be $\mathcal{O}(NK)$ different relative positions of $(\mathbf{c}_i - \mathbf{c}_j)$ for possible (i, j) pairs due to the continuity of \mathbf{c} .

Reducing space complexity. We introduce a coordinate decomposition approach to reduce space complexity. Given a query voxel $(\mathbf{v}_i, \mathbf{f}_i, \mathbf{c}_i)$ and a key voxel $(\mathbf{v}_j, \mathbf{f}_j, \mathbf{c}_j)$, the relative position of centroids $\mathbf{c}_i - \mathbf{c}_j$ can be decomposed as follows:

$$\mathbf{c}_i - \mathbf{c}_j = (\mathbf{c}_i - \mathbf{v}_i) - (\mathbf{c}_j - \mathbf{v}_j) + (\mathbf{v}_i - \mathbf{v}_j). \quad (5)$$

With Eq. (5), we can decompose the memory-consuming $\delta(\mathbf{c}_i, \mathbf{c}_j)$ into two kinds of positional encodings: (1) a continuous positional encoding $\delta_{\text{abs}}(\mathbf{c}_i - \mathbf{v}_i)$ whose space complexity is $\mathcal{O}(ND)$ due to continuity of \mathbf{c} , and (2) a discretized positional encoding $\delta_{\text{rel}}(\mathbf{v}_i - \mathbf{v}_j)$ whose space complexity is $\mathcal{O}(KD)$. $\delta_{\text{rel}}(\mathbf{v}_i - \mathbf{v}_j)$ is memory-efficient because there can be only K different discretized relative positions of $(\mathbf{v}_i - \mathbf{v}_j) \in \mathbb{R}^3$ for all possible (i, j) pairs. In addition, it is due to the fact that the K is a way smaller than number of points N . $\delta_{\text{abs}}(\mathbf{c}_j - \mathbf{v}_j)$ in Eq. (5) does not add any additional space complexity because we already have $\delta_{\text{abs}}(\mathbf{c}_i - \mathbf{v}_i)$ for every voxel. As a result, space complexity of $\delta(\mathbf{c}_i, \mathbf{c}_j)$ become $\mathcal{O}(NKD)$ to $\mathcal{O}(ND + KD)$.

Given, Eq. (4) and (5), we see that local self-attention use continuous positional encoding $\delta_{\text{abs}}(\mathbf{c}_i - \mathbf{v}_i)$ and input voxel feature \mathbf{f}_i . Therefore, the local self-attention pipeline has *centroid-aware* property that can reduce quantization artifacts. Based on these insights, we propose to use an aggregated feature $\mathbf{g}_i = \mathbf{f}_i + \delta_{\text{abs}}(\mathbf{c}_i - \mathbf{v}_i)$ and name it as *centroid-aware* voxel feature. We compute attention weights

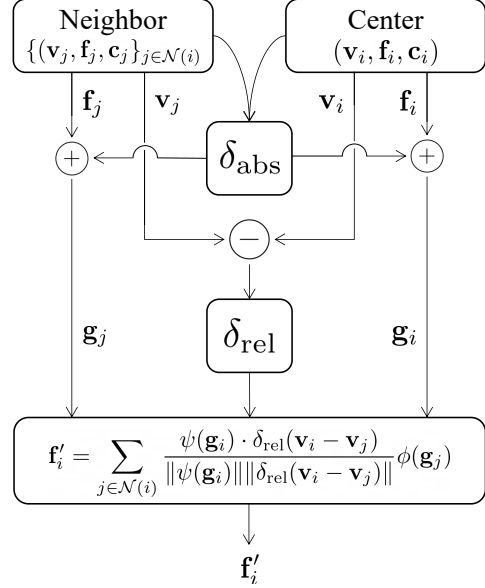


Figure 3. **Computational Graph.** We illustrate the overall computation procedures of our proposed model with the form of a computational graph.

with $\delta_{\text{rel}}(\mathbf{v}_i - \mathbf{v}_j)$ as follows:

$$\mathbf{f}'_i = \sum_{j \in \mathcal{N}(i)} a(\mathbf{g}_i, \delta_{\text{rel}}(\mathbf{v}_i - \mathbf{v}_j)) \psi(\mathbf{g}_j). \quad (6)$$

Lightweight Self-Attention Layer. Now, we propose the new local self-attention layer, named LSA layer, by defining attention function $a(\cdot)$ in Eq. (6) as follows:

$$\mathbf{f}'_i = \sum_{j \in \mathcal{N}(i)} \frac{\psi(\mathbf{g}_i) \cdot \delta_{\text{rel}}(\mathbf{v}_i - \mathbf{v}_j)}{\|\psi(\mathbf{g}_i)\| \|\delta_{\text{rel}}(\mathbf{v}_i - \mathbf{v}_j)\|} \phi(\mathbf{g}_j). \quad (7)$$

It is worth noting that LSA layer use the *cosine similarity* between $\psi(\mathbf{g}_i)$ and $\delta_{\text{rel}}(\mathbf{v}_i - \mathbf{v}_j)$. Instead of using $\text{softmax}(\psi(\mathbf{g}_i)^\top \delta_{\text{rel}}(\mathbf{v}_i - \mathbf{v}_j))$, cosine similarity can effectively handle the sparsity issue of input voxels \mathcal{V} properly. For an example, an issue arises if we use $\text{softmax}(\cdot)$ and $|\mathcal{N}(i)|$ is 1. In this case, $\text{softmax}(\cdot)$ normalizes the attention weights into 1.0, and it can make the LSA layer to be a simple linear layer ϕ . In addition, as the LSA layer queries local neighbor indices, $|\mathcal{N}(i)|$ varies from 1 to the number of neighboring voxels. Therefore, *cosine similarity* is more natural choice for handling varying number of voxels than $\text{softmax}(\cdot)$ as shown in Table 6.

As shown in Figure 3, the dynamics of LSA layer (Eq. (7)) generates weights using the *centroid-aware* features $\psi(\mathbf{g}_i)$ and relative voxel features $\delta_{\text{rel}}(\mathbf{v}_i - \mathbf{v}_j)$. This design enables LSA layer to learn more coherent representation under the rigid transformations than sparse convolution based approach [5], as shown in Table 1 and to outperform sparse convolution on various tasks (e.g., 3D semantic segmentation,

3D object detection) as shown in Table 2, Table 3, and Table 8. We also experimentally show that the reformulation from Eq. (4) to Eq. (6) works reasonably. (as shown in Table 5 and Table 6) and introduces extra efficiency (as shown in Table 2).

3.4. Network Architecture

We develop Fast Point Transformer for dense prediction on point cloud based on the modules introduced above. Using coordinate hashing (Sec. 3.2) and decomposed positional encodings (Sec. 3.3), Fast Point Transformer is less prone to quantization errors than previous voxel-based methods [5, 9, 21], while also being significantly more faster than point-based methods [38, 46] in terms of both space and time. Furthermore, the proposed local self-attention layer can be easily be *integrated to voxel-based downsampling and upsampling layer* without introducing heuristic sampling and grouping mechanism like most of the point-based methods [24, 38, 46]. Note that we can build local self-attention networks by substituting convolution layers with LSA layers. Therefore, any successful sparse CNN architectures can be modified to facilitate local self-attention, e.g., ResNet [12] and U-Net [28]. We implement our model for semantic segmentation using the U-Net [28] architecture. Further details are described in the supplement.

4. Experiments

In this section, we evaluate our model on two popular large-scale 3D scene datasets: S3DIS [1] and ScanNet [6]. We have selected the two datasets due to their rich diversity and densely annotated labels. We first validate the robustness of our approach to voxel hashing configurations described in Sec. 4.3. Then, we compare the proposed method with the state-of-the-art and discuss the results in Sec. 4.4 and Sec. 4.5. We have conducted all experiments with a fixed random seed for reproducibility. We have described details (e.g., hyperparameters, learning rate) of all the experiments in the supplement.

4.1. Datasets

S3DIS is a large-scale indoor dataset which consists of six large-scale areas with 271 room scenes. We test on Area 5 and utilize the other splits during training. Following [5], we do not use any preprocessing methods e.g., *cropping into small blocks* that are widely used in point-based methods [16, 17, 23, 32, 33, 38].

ScanNet. We use the second official release of ScanNet [6], which consists of 1.5k room scenes with some rooms captured repeatedly with different sensors. Following the experimental settings of prior work [3, 22], our model uses point-wise RGB colors as input point features $\{\mathbf{i}_n\}$ for 3D semantic segmentation task and 3D objection detection, respectively.

4.2. Baselines

We have selected PointNet [23], PointWeb [45], SP-Graph [16], PointConv [37], PointASNL [39], KP-Conv [34], PAConv [38], Point Transformer [46], SparseConvNet [9], and MinkowskiNet [5] as the baseline approaches. MinkowskiNet32 and MinkowskiNet42 [5] are compared as representative voxel-based methods that comprise 32 and 42 U-Net layers, respectively. We reproduce MinkowskiNet42 [5] with the official source code and denote it as MinkowskiNet42[†] with different voxel sizes. PointNet [23], SPGraph [16], PointWeb [45], KPConv [34], PAConv [38] and Point Transformer [46] are selected since they are representative point-based methods. The main difference between KPConv [34] and the others is that KPConv [34] uses a k -d tree to boost its inference time while the others do not. We follow the official guideline of the methods and reproduce the results. A most recent method, Point Transformer [46] has also been selected due to its superiority on several datasets. Unlike our method and selected baselines, other approaches [4, 14, 15] use additional inputs e.g., 2D images or meshes. Accordingly, we have excluded these methods from the comparison.

4.3. Consistency Test

We introduce a new evaluation metric to measure the coherency of predictions under various rigid transformations, such as translation and rotation. Let us consider a set of point clouds $\mathcal{S} = \{\mathcal{P}^{\text{in}}\}$ and a 3D semantic segmentation model $f : \mathcal{P}^{\text{in}} \mapsto \mathbb{C}$ which predicts a semantic class of each point in $\mathcal{P}^{\text{in}} = \{(\mathbf{p}_n, \mathbf{i}_n)\}$. Given \mathcal{S} and a set of rigid transformations $\mathcal{T} = \{\mathbf{T}_m\}$, we introduce the consistency score (CScore($f; \mathcal{S}, \mathcal{T}$)) as follows:

$$\frac{1}{|\mathcal{S}|} \sum_{\mathcal{P}^{\text{in}} \in \mathcal{S}} \frac{1}{|\mathcal{P}^{\text{in}}||\mathcal{T}|} \sum_n \sum_m \mathbb{I}(f(\mathbf{p}_n, \mathbf{i}_n), f(\mathbf{T}_m \mathbf{p}_n, \mathbf{i}_n)), \quad (8)$$

where $\mathbb{I}(\cdot)$ is the indicator function, and it checks whether class predictions of the original point and the transformed point are the same. CScore is an averaged accuracy over \mathcal{S} , \mathcal{P} , and \mathcal{T} . Similarly, we use the point-wise CScore of f on \mathcal{P} to show which points in \mathcal{P} is vulnerable to \mathcal{T} . We apply 41 different rigid transformations that consist of 26 translations and 15 rotations around the gravity axis. For the voxel size L , 26 translations are set to $[0, L/3, 2L/3]^3$ except zero translation $[0, 0, 0]$. Fifteen rotation angles along gravity axis is set to $[0, 0.125\pi, 0.25\pi, \dots, 1.875\pi]$. We evaluate CScore of MinkowskiNet42 and Fast Point Transformer on ScanNet validation split. The evaluation results (Table 1) and the qualitative results (Figure 4) show that Fast Point Transformer outputs more coherent feature representations than MinkowskiNet42 [5]. Moreover, the coherent predic-

Table 1. **Comparison of consistency scores.** We compare the consistency scores of Fast Point Transformer and MinkowskiNet42[†], which is the reproduced model, on different transformation sets. The transformation sets are 1) rotation only (**R**), 2) translation only (**t**), and 3) both (**R** and **t**). The size of voxel is set to 10cm, 5cm, and 2cm in a ScanNet dataset. Fast Point Transformer relieves the prediction inconsistency that occurred by voxelization artifact.

Methods	CScore (%)			mIoU (%)
	R	t	R and t	
<i>Voxel size: 10cm</i>				
MinkowskiNet42 [†]	72.8	71.7	72.1	60.4
FastPointTransformer (ours)	76.5	73.5	74.6	65.3
<i>Voxel size: 5cm</i>				
MinkowskiNet42 [†]	74.5	74.8	74.7	66.6
FastPointTransformer (ours)	85.2	77.5	80.3	70.1
<i>Voxel size: 2cm</i>				
MinkowskiNet42 [†]	96.3	96.7	96.6	71.7
FastPointTransformer (ours)	97.2	97.1	97.1	72.0



Figure 4. **Heatmap visualization of Consistency Score (CScore).** We visualize consistency scores of MinkowskiNet [5] and the proposed efficient point transformer with the hot heatmap. Points with high CScore (consistently predicts the same class) are colored black, and points with low CScore (the predicted class is not consistent with arbitrary rigid transformations) are colored white. Table 1 shows quantitative evaluation.

tions indicate that the Fast Point Transformer successfully relieves quantization artifacts.

4.4. 3D Semantic Segmentation

We compare our approach with the state of the arts on S3DIS and ScanNet. We use the mean of class-wise IoU scores as the primary evaluation metric for both datasets.

S3DIS. We compare the computational complexity, the mean accuracy, and the mean IoU of Fast Point Transformer with the state of the arts on the S3DIS Area 5 test split. Since Choy et al. [5] reported results with a lightweight network (MinkowskiNet32) at voxel size 5cm, we utilize the official code of MinkowskiNet42 and reproduce the results denoted by MinkowskiNet42[†] with the same voxel size.

Table 2 theoretically analyzes the time complexity and reports the average wall-time latency of each method when processing S3DIS Area 5 scenes. We measure the inference time of MinkowskiNet42[†], PointNet [23], SPGraph [16], PointWeb [45], KPConv [34], PACConv [38], and Point Transformer [46] using the official codes. We use the same ma-

chine with Intel(R) Core(TM) i7-5930K CPU and a single NVIDIA Geforce RTX 3090 GPU to measure the latency of methods. Detailed information about the time complexity analysis is included in the supplement.

Due to the preprocessing stage and stitching the multiple local predictions [16, 23, 38, 45] or multiple inferences [34, 46], the point-based methods take much more time to inference a single scene than our approach. Note that KPConv [34] constructs k -d tree, but we do not include this process into inference time. Our Fast Point Transformer processes a large-scale scene at least 87 times faster than point-based methods [16, 23, 34, 38, 45, 46] as shown in Table 2. Specifically, PointNet [23] takes 18.16 seconds for processing a scene on average because it crops the scene into $1m \times 1m \times 1m$ blocks, predicts on the blocks, and stitches the predictions for the scene-level prediction (denoted by ‘Crop-and-stitch’ in Table 2). Moreover, Fast Point Transformer outperforms MinkowskiNet42[†] by 1.5 absolute percentage score in mean IoU (%) with a comparable speed. Given the reported results by Zhao et al. [46], Point Transformer shows the best accuracy. However, Point Transformer [46] shows 136 times slower inference speed than our approach. This is because it grid-subsamples points and infers the sampled points multiple times with the expensive k nearest neighbor search to cover the whole scene (denoted by ‘Multi-shot’ in Table 2), while our approach can handle the whole scene with a single feed-forward operation (denoted by ‘Single-shot’ in Table 2).

ScanNet. We evaluate the models on the ScanNet validation split due to strict submission policies of ScanNet online test benchmark, where one method can be tested at most once. Our proposed method outperforms MinkowskiNet42[†] at voxel sizes of 2cm, 5cm, and 10cm by 0.3, 3.5, and 4.9 absolute percentage point gain in Mean IoU (%) respectively. The experimental results in Table 1 and Table 3 indicate that the proposed method can represent a large-scale point cloud as features that are more robust to quantization error.

mIoU vs. model size. We compare the accuracy of both Fast Point Transformer and MinkowskiNet with the different number of parameters. We build small network models by maintaining the number of building blocks as MinkowskiNet [5] does and reducing the number of channels. Detailed illustration about network architecture is shown in the supplement. Table 4 shows the evaluation results.

Interestingly, we observe that Fast Point Transformer is more resilient to the network parameter reduction, and Fast Point Transformer models outperform their counterpart models of MinkowskiNet. We can observe that the most lightweight Fast Point Transformer with voxel size 10cm outperforms the most lightweight MinkowskiNet [5] with voxel size 5cm. MinkowskiNet [5] requires lots of parameters to overcome voxelization artifacts, whereas Fast Point Transformer shows a consistent accuracy even with 71.5%

Table 2. **3D semantic segmentation on S3DIS [1] Area 5 test.** We mark the reproduced models using the official source codes as \dagger . We analyze the theoretical time complexity of neighbor search algorithms and evaluate the per-scene wall-time latency of each network. We denote N as the number of dataset points, M as the number of query points, and K as the number of neighbors to search. Both M and N are much larger than K in a large-scale point cloud.

Methods	Neighbor Search		Large-scale Inference	Latency (Seconds)	Latency (Normalized)	mAcc (%)	mIoU (%)
	Preparation	Inference					
PointNet [23]	\times	\times	Crop-and-stitch	18.16	136.54	49.0	41.1
SPGraph [16]	\times	\times	Crop-and-stitch	18.28	137.44	66.5	58.0
PointWeb [45]	$\mathcal{O}(1)$	$\mathcal{O}(MNK)$	Crop-and-stitch	11.62	87.37	66.6	60.3
KPConv <i>deform</i> [34]	$\mathcal{O}(N \log N)$	$\mathcal{O}(KM \log N)$	Multi-shot	105.15	760.53	72.8	67.1
PACConv [38]	$\mathcal{O}(1)$	$\mathcal{O}(MN \log K)$	Crop-and-stitch	28.13	211.50	73.0	66.6
PointTransformer [46]	$\mathcal{O}(1)$	$\mathcal{O}(MN \log K)$	Multi-shot	18.07	135.87	76.5	70.4
<i>Voxel size: 5cm</i>							
MinkowskiNet32 [5]	$\mathcal{O}(N)$	$\mathcal{O}(M)$	Single-shot	0.08	0.62	71.7	65.4
MinkowskiNet42 \dagger	$\mathcal{O}(N)$	$\mathcal{O}(M)$	Single-shot	0.07	0.54	73.3	66.0
+ rotation average	$\mathcal{O}(N)$	$\mathcal{O}(M)$	Multi-shot	0.57	4.38	73.5	67.1
FastPointTransformer (ours)	$\mathcal{O}(N)$	$\mathcal{O}(M)$	Single-shot	0.13	1.00	74.7	67.5
+ rotation average	$\mathcal{O}(N)$	$\mathcal{O}(M)$	Multi-shot	1.05	8.08	75.5	68.5

Table 3. **3D semantic segmentation.** We mark the reproduced models using the official source codes as \dagger . We use ScanNet [6] validation set.

Methods	mIoU (%)
PointNet [23]	53.5
PointConv [37]	61.0
PointASNL [39]	63.5
KPConv <i>deform</i> [34]	69.2
<i>Voxel size: 2cm</i>	
SparseConvNet [9]	69.3
MinkowskiNet42 [5]	72.2
MinkowskiNet42 \dagger	71.7
FastPointTransformer (ours)	72.0

fewer network parameters.

These results imply that the proposed lightweight self-attention (LSA) layer can learn a 3D geometry more effectively than an over-parameterized sparse convolutional layer thanks to its dynamic kernel weights with the proposed positional encodings.

Ablation study. We conduct ablation studies on (1) the proposed positional encodings, (2) attention types, and (3) the local window size. We use the ScanNet validation dataset for the experiments. We have followed the same setup with the main experiments with a voxel size of 10cm.

Table 5 shows ablation results on the proposed positional encodings, *i.e.*, δ_{enc} and δ_{abs} . Models with full positional encodings achieved the best mIoU score. When removing δ_{abs} from our model, we have observed a large performance drop since the model does not adopt continuous position information. Removing either positional encodings of *centroid-aware* voxelization or devoxelization from our network also degrades the performance. These results indicate that both proposed voxelization and devoxelization effectively main-

Table 4. **mIoU vs. model size.** Under reduced number of network parameters, Fast Point Transformer shows little performance drop while MinkowskiNet [5] shows gradual degrades. We color green for the **positive changes** and red for the **negative changes** w.r.t. the base model. We use ScanNet [6] validation set for the experiment.

Methods	# Param. (M)		mIoU (%)	
		Rel. (%)		Δ
<i>Voxel size: 10cm</i>				
MinkowskiNet42 \dagger	37.9	± 0.0	60.4	± 0.0
MinkowskiNet (small)	21.7	$\downarrow 42.7$	59.2	$\downarrow 0.8$
MinkowskiNet (smaller)	11.6	$\downarrow 69.4$	57.2	$\downarrow 3.2$
FastPointTransformer (ours)	37.9	± 0.0	65.3	± 0.0
FastPointTransformer (small)	20.2	$\downarrow 46.7$	65.7	$\uparrow 0.4$
FastPointTransformer (smaller)	10.8	$\downarrow 71.5$	65.6	$\uparrow 0.3$
<i>Voxel size: 5cm</i>				
MinkowskiNet42 \dagger	37.9	± 0.0	66.6	± 0.0
MinkowskiNet (small)	21.7	$\downarrow 42.7$	65.9	$\downarrow 0.7$
MinkowskiNet (smaller)	11.6	$\downarrow 69.4$	63.9	$\downarrow 2.7$
FastPointTransformer (ours)	37.9	± 0.0	70.1	± 0.0
FastPointTransformer (small)	20.2	$\downarrow 46.7$	70.1	± 0.0
FastPointTransformer (smaller)	10.8	$\downarrow 71.5$	69.9	$\downarrow 0.2$

tain continuous geometric information of the input point cloud. Moreover, the proposed positional encodings also improve the performance of MinkowskiNet42 \dagger although the total number of parameters becomes much bigger than Fast Point Transformer. However, additional usage of δ_{abs} does not improve the performance of MinkowskiNet42 [5], which means that the self-attention mechanism is a more proper way to use δ_{abs} than sparse convolution.

Table 6 shows the effects of attention types used in the proposed LSA layer. $\text{cosine}(\cdot)$ handles the varying number of neighbors more effectively than $\text{softmax}(\cdot)$ as shown in Table 6. However, as reported in local self-attention litera-

Table 5. **Ablation study on the proposed positional encodings.** Note that Mink42[†] and FastPointTrans. denote MinkowskiNet42[†] and Fast Point Transformer, respectively.

	# Param. (M)	δ_{enc}		δ_{abs}	mIoU (%)
		Vox	Devox		
Mink42 [†]	37.9				60.4
	38.0	✓			63.2
	38.0	✓	✓		65.1
	51.6	✓	✓	✓	65.0
FastPointTrans.	27.3				59.1
	27.3	✓			61.3
	37.8			✓	62.1
	27.3	✓	✓		62.7
	37.8	✓		✓	63.4
	37.9	✓	✓	✓	65.3

Table 6. **Ablation study on attention types.**

$a(\cdot)$ in Eq. (6)	mIoU (%)
$\text{softmax}(\psi(\mathbf{g}_i), \delta_{\text{rel}}(\mathbf{v}_i - \mathbf{v}_j))$	61.0
$\text{cosine}(\psi(\mathbf{g}_i), \xi(\mathbf{g}_j) + \delta_{\text{rel}}(\mathbf{v}_i - \mathbf{v}_j))$	62.1
$\text{cosine}(\psi(\mathbf{g}_i), \delta_{\text{rel}}(\mathbf{v}_i - \mathbf{v}_j))$	65.3

Table 7. **Ablation study on the local window size.** k is the local window size used to find the neighbors, $\mathcal{N}(i)$, in Eq. (7).

k	Latency (sec)	mIoU (%)
3	0.106	65.3
5	0.127	62.4
7	0.168	61.9

ture [2, 26], additional usage of the similarity between query $\psi(\mathbf{g}_i)$ and key $\xi(\mathbf{g}_j)$ does not improve the performance of the proposed LSA layer.

In Table 7, we show the effect of the local window size in the proposed LSA layer. Since we currently use learnable tokens for $\delta_{\text{rel}}(\mathbf{v}_i - \mathbf{v}_j)$, increasing the local window size degrades the performance due to the sparsity of 3D data. Introducing an inductive bias, such as concatenating the positional encodings [26] or a shared mapping layer [46] can be one of the possible solutions.

4.5. 3D Object Detection

We have conducted experiments on ScanNet 3D object detection dataset, where fine-grained point cloud representation is essential to detect and localize 3D objects.

Setup. For a fair comparison of Fast Point Transformer with previously proposed methods [5, 24], we use TorchPoints3D, an open-source library implemented by Chaton et al. [3] for reproducible deep learning on 3D point clouds. TorchPoints3D sub-samples a fixed number of points from an input point cloud which is widely used for PointNet++ [24] to process a scene-level point cloud-like ScanNet. We notice that the library also sub-sample points

Table 8. **3D object detection on ScanNet [6].** We report two mAP scores of VoteNet [22] with different backbones on ScanNet [6] dataset. Numbers except that of MinkowskiNet[†] and Fast Point Transformer are taken from Chaton et al. [3].

Backbones	mAP@0.25	mAP@0.50
PointNet++ [24]	54.2	30.1
RS-CNN [18]	51.6	29.5
KPConv [34]	48.9	29.2
MinkowskiNet [5]	53.8	30.2
MinkowskiNet [†]	55.3	32.8
FastPointTransformer (ours)	59.1	35.3

for the voxel-based methods, such as MinkowskiNet [5], which is not a suitable experimental configuration. Therefore, we reproduce VoteNet with MinkowskiNet backbone, which is denoted by MinkowskiNet[†] in Table 8 without input point sub-sampling, and we use the original experimental configurations. In addition, we train a new VoteNet [22] with the Fast Point Transformer backbone without any change of detection network architecture (e.g., voting module). Further details are included in the supplement.

Results. As shown in Table 8, the VoteNet [22] model with Fast Point Transformer as a backbone outperforms other baselines with a large margin. The results show that the proposed continuous positional encodings that Fast Point Transformer uses can effectively encode point cloud representation and help the 3D detection task.

5. Limitation

Our Fast Point Transformer is made to get benefits of point-based methods [17, 23, 24, 37, 39, 45, 46] (utilizing continuous coordinates) and voxel-based methods [5, 9, 21, 47] (fast inference time). Although our model successfully relieves quantization artifacts without expensive computational costs, unlike previous works [19, 31, 42], there is still room for improvement. Developing a fully quantization-free voxelization and devoxelization would improve the performance of Fast Point Transformer with smaller voxel sizes.

6. Conclusion

We have introduced the Fast Point Transformer and demonstrated its speed and accuracy on 3D semantic segmentation and 3D detection tasks. The experimental results on large-scale 3D datasets show that our approach is competitive to the best voxel-based method [5], and our network achieves 136 times faster inference time than the state-of-the-art, Point Transformer, with a reasonable accuracy trade-off. In the future, we will explore architectures for Fast Point Transformer rather than U-shaped architectures [28] because the U-shaped network is initially designed for convolutional layers. Our code and data are going to be publicly available.

References

- [1] Iro Armeni, Ozan Sener, Amir R Zamir, Helen Jiang, Ioannis Brilakis, Martin Fischer, and Silvio Savarese. 3d semantic parsing of large-scale indoor spaces. In *Proceedings of the IEEE Conference on Computer Vision and Pattern Recognition*, pages 1534–1543, 2016. [2](#), [5](#), [7](#), [11](#), [14](#)
- [2] Irwan Bello. Lambdanetworks: Modeling long-range interactions without attention. In *International Conference on Learning Representations*, 2021. [2](#), [3](#), [8](#)
- [3] Thomas Chaton, Nicolas Chaulet, Sofiane Horache, and Loic Landrieu. Torch-points3d: A modular multi-task framework for reproducible deep learning on 3d point clouds. In *2020 International Conference on 3D Vision (3DV)*, pages 1–10. IEEE, 2020. [5](#), [8](#)
- [4] Hung-Yueh Chiang, Yen-Liang Lin, Yueh-Cheng Liu, and Winston H Hsu. A unified point-based framework for 3d segmentation. In *2019 International Conference on 3D Vision (3DV)*, pages 155–163. IEEE, 2019. [5](#)
- [5] Christopher Choy, JunYoung Gwak, and Silvio Savarese. 4d spatio-temporal convnets: Minkowski convolutional neural networks. In *CVPR*, pages 3075–3084, 2019. [1](#), [2](#), [3](#), [4](#), [5](#), [6](#), [7](#), [8](#), [11](#), [12](#), [13](#), [14](#), [15](#)
- [6] Angela Dai, Angel X Chang, Manolis Savva, Maciej Halber, Thomas Funkhouser, and Matthias Nießner. Scannet: Richly-annotated 3d reconstructions of indoor scenes. In *CVPR*, pages 5828–5839, 2017. [2](#), [5](#), [7](#), [8](#), [11](#), [13](#)
- [7] Jacob Devlin, Ming-Wei Chang, Kenton Lee, and Kristina Toutanova. Bert: Pre-training of deep bidirectional transformers for language understanding. *arXiv preprint arXiv:1810.04805*, 2018. [2](#)
- [8] Alexey Dosovitskiy, Lucas Beyer, Alexander Kolesnikov, Dirk Weissenborn, Xiaohua Zhai, Thomas Unterthiner, Mostafa Dehghani, Matthias Minderer, Georg Heigold, Sylvain Gelly, et al. An image is worth 16x16 words: Transformers for image recognition at scale. *arXiv preprint arXiv:2010.11929*, 2020. [2](#)
- [9] Benjamin Graham, Martin Engelcke, and Laurens Van Der Maaten. 3d semantic segmentation with submanifold sparse convolutional networks. In *CVPR*, pages 9224–9232, 2018. [1](#), [2](#), [3](#), [5](#), [7](#), [8](#)
- [10] Meng-Hao Guo, Jun-Xiong Cai, Zheng-Ning Liu, Tai-Jiang Mu, Ralph R Martin, and Shi-Min Hu. Pct: Point cloud transformer. *arXiv preprint arXiv:2012.09688*, 2020. [2](#), [3](#)
- [11] Kai Han, An Xiao, Enhua Wu, Jianyuan Guo, Chunjing Xu, and Yunhe Wang. Transformer in transformer. *arXiv preprint arXiv:2103.00112*, 2021. [2](#)
- [12] Kaiming He, Xiangyu Zhang, Shaoqing Ren, and Jian Sun. Deep residual learning for image recognition. In *Proceedings of the IEEE conference on computer vision and pattern recognition*, pages 770–778, 2016. [5](#)
- [13] Han Hu, Zheng Zhang, Zhenda Xie, and Stephen Lin. Local relation networks for image recognition. In *Proceedings of the IEEE/CVF International Conference on Computer Vision*, pages 3464–3473, 2019. [11](#)
- [14] Wenbo Hu, Hengshuang Zhao, Li Jiang, Jiaya Jia, and Tien-Tsin Wong. Bidirectional projection network for cross dimension scene understanding. *arXiv preprint arXiv:2103.14326*, 2021. [5](#)
- [15] Abhijit Kundu, Xiaoqi Yin, Alireza Fathi, David Ross, Brian Brewington, Thomas Funkhouser, and Caroline Pantofaru. Virtual multi-view fusion for 3d semantic segmentation. In *European Conference on Computer Vision*, pages 518–535. Springer, 2020. [5](#)
- [16] Loic Landrieu and Martin Simonovsky. Large-scale point cloud semantic segmentation with superpoint graphs. In *Proceedings of the IEEE Conference on Computer Vision and Pattern Recognition*, pages 4558–4567, 2018. [5](#), [6](#), [7](#), [11](#), [13](#), [14](#)
- [17] Yangyan Li, Rui Bu, Mingchao Sun, Wei Wu, Xinhan Di, and Baoquan Chen. Pointcnn: Convolution on χ -transformed points. In *Proceedings of the 32nd International Conference on Neural Information Processing Systems*, pages 828–838, 2018. [1](#), [5](#), [8](#)
- [18] Yongcheng Liu, Bin Fan, Shiming Xiang, and Chunhong Pan. Relation-shape convolutional neural network for point cloud analysis. In *CVPR*, pages 8895–8904, 2019. [8](#)
- [19] Zhijian Liu, Haotian Tang, Yujun Lin, and Song Han. Point-voxel cnn for efficient 3d deep learning. In *NeurIPS*, 2019. [1](#), [2](#), [8](#)
- [20] Jiageng Mao, Xiaogang Wang, and Hongsheng Li. Interpolated convolutional networks for 3d point cloud understanding. In *ICCV*, October 2019. [1](#), [2](#)
- [21] Jiageng Mao, Yujing Xue, Minzhe Niu, Haoyue Bai, Jiashi Feng, Xiaodan Liang, Hang Xu, and Chunjing Xu. Voxel transformer for 3d object detection. *arXiv preprint arXiv:2109.02497*, 2021. [1](#), [2](#), [3](#), [5](#), [8](#)
- [22] Charles R Qi, Or Litany, Kaiming He, and Leonidas J Guibas. Deep hough voting for 3d object detection in point clouds. In *Proceedings of the IEEE/CVF International Conference on Computer Vision*, pages 9277–9286, 2019. [2](#), [5](#), [8](#), [15](#)
- [23] Charles R Qi, Hao Su, Kaichun Mo, and Leonidas J Guibas. Pointnet: Deep learning on point sets for 3d classification and segmentation. In *CVPR*, pages 652–660, 2017. [1](#), [2](#), [5](#), [6](#), [7](#), [8](#), [11](#), [13](#), [14](#)
- [24] Charles R Qi, Li Yi, Hao Su, and Leonidas J Guibas. Pointnet++ deep hierarchical feature learning on point sets in a metric space. In *CVPR*, pages 5105–5114, 2017. [1](#), [2](#), [5](#), [8](#)
- [25] Alec Radford, Karthik Narasimhan, Tim Salimans, and Ilya Sutskever. Improving language understanding by generative pre-training. 2018. [2](#)
- [26] Prajit Ramachandran, Niki Parmar, Ashish Vaswani, Irwan Bello, Anselm Levskaya, and Jonathon Shlens. Stand-alone self-attention in vision models. *arXiv preprint arXiv:1906.05909*, 2019. [2](#), [3](#), [8](#)
- [27] Prajit Ramachandran, Niki Parmar, Ashish Vaswani, Irwan Bello, Anselm Levskaya, and Jonathon Shlens. Stand-alone self-attention in vision models. In H. Wallach, H. Larochelle, A. Beygelzimer, F. d'Alché-Buc, E. Fox, and R. Garnett, editors, *Advances in Neural Information Processing Systems*, volume 32. Curran Associates, Inc., 2019. [4](#)
- [28] Olaf Ronneberger, Philipp Fischer, and Thomas Brox. U-net: Convolutional networks for biomedical image segmentation. In *International Conference on Medical image computing and computer-assisted intervention*, pages 234–241. Springer, 2015. [5](#), [8](#)
- [29] Radu Alexandru Rosu, Peer Schütt, Jan Quenzel, and Sven Behnke. Latticenet: Fast point cloud segmentation using permutohedral lattices. *arXiv preprint arXiv:1912.05905*,

2019. [3](#)
- [30] Hang Su, Varun Jampani, Deqing Sun, Subhansu Maji, Evangelos Kalogerakis, Ming-Hsuan Yang, and Jan Kautz. Splatnet: Sparse lattice networks for point cloud processing. In *Proceedings of the IEEE conference on computer vision and pattern recognition*, pages 2530–2539, 2018. [3](#)
- [31] Haotian Tang, Zhijian Liu, Shengyu Zhao, Yujun Lin, Ji Lin, Hanrui Wang, and Song Han. Searching efficient 3d architectures with sparse point-voxel convolution. In *ECCV*, pages 685–702. Springer, 2020. [1](#), [2](#), [8](#)
- [32] Maxim Tatarchenko, Jaesik Park, Vladlen Koltun, and Qian-Yi Zhou. Tangent convolutions for dense prediction in 3d. In *Proceedings of the IEEE Conference on Computer Vision and Pattern Recognition*, pages 3887–3896, 2018. [1](#), [5](#)
- [33] Lyne Tchapmi, Christopher Choy, Iro Armeni, JunYoung Gwak, and Silvio Savarese. Segcloud: Semantic segmentation of 3d point clouds. In *2017 international conference on 3D vision (3DV)*, pages 537–547. IEEE, 2017. [1](#), [5](#)
- [34] Hugues Thomas, Charles R Qi, Jean-Emmanuel Deschaud, Beatriz Marcotegui, François Goulette, and Leonidas J Guibas. Kpconv: Flexible and deformable convolution for point clouds. In *ICCV*, pages 6411–6420, 2019. [1](#), [2](#), [5](#), [6](#), [7](#), [8](#), [11](#), [12](#), [13](#), [14](#)
- [35] Ashish Vaswani, Prajit Ramachandran, Aravind Srinivas, Niki Parmar, Blake Hechtman, and Jonathon Shlens. Scaling local self-attention for parameter efficient visual backbones. *arXiv preprint arXiv:2103.12731*, 2021. [2](#), [3](#)
- [36] Ashish Vaswani, Noam Shazeer, Niki Parmar, Jakob Uszkoreit, Llion Jones, Aidan N Gomez, Łukasz Kaiser, and Illia Polosukhin. Attention is all you need. *arXiv preprint arXiv:1706.03762*, 2017. [2](#)
- [37] Wenxuan Wu, Zhongang Qi, and Li Fuxin. Pointconv: Deep convolutional networks on 3d point clouds. In *Proceedings of the IEEE/CVF Conference on Computer Vision and Pattern Recognition*, pages 9621–9630, 2019. [5](#), [7](#), [8](#)
- [38] Mutian Xu, Runyu Ding, Hengshuang Zhao, and Xiaojuan Qi. Paconv: Position adaptive convolution with dynamic kernel assembling on point clouds. *arXiv preprint arXiv:2103.14635*, 2021. [1](#), [4](#), [5](#), [6](#), [7](#), [11](#), [12](#), [13](#), [14](#)
- [39] Xu Yan, Chaoda Zheng, Zhen Li, Sheng Wang, and Shuguang Cui. Pointasnl: Robust point clouds processing using nonlocal neural networks with adaptive sampling. In *Proceedings of the IEEE/CVF Conference on Computer Vision and Pattern Recognition*, pages 5589–5598, 2020. [5](#), [7](#), [8](#)
- [40] Li Yuan, Yunpeng Chen, Tao Wang, Weihao Yu, Yujun Shi, Zihang Jiang, Francis EH Tay, Jiashi Feng, and Shuicheng Yan. Tokens-to-token vit: Training vision transformers from scratch on imagenet. *arXiv preprint arXiv:2101.11986*, 2021. [2](#)
- [41] Cheng Zhang, Haocheng Wan, Shengqiang Liu, Xinyi Shen, and Zizhao Wu. Pvt: Point-voxel transformer for 3d deep learning, 2021. [2](#)
- [42] Feihu Zhang, Jin Fang, Benjamin Wah, and Philip Torr. Deep fusionnet for point cloud semantic segmentation. In *ECCV*, volume 2, page 6, 2020. [2](#), [3](#), [8](#)
- [43] Richard Zhang. Making convolutional networks shift-invariant again. In *International conference on machine learning*, pages 7324–7334. PMLR, 2019. [2](#)
- [44] Hengshuang Zhao, Jiaya Jia, and Vladlen Koltun. Exploring self-attention for image recognition. In *Proceedings of the IEEE/CVF Conference on Computer Vision and Pattern Recognition (CVPR)*, June 2020. [4](#)
- [45] Hengshuang Zhao, Li Jiang, Chi-Wing Fu, and Jiaya Jia. Pointweb: Enhancing local neighborhood features for point cloud processing. In *Proceedings of the IEEE/CVF Conference on Computer Vision and Pattern Recognition*, pages 5565–5573, 2019. [5](#), [6](#), [7](#), [8](#), [11](#), [12](#), [13](#), [14](#)
- [46] Hengshuang Zhao, Li Jiang, Jiaya Jia, Philip Torr, and Vladlen Koltun. Point transformer, 2021. [1](#), [2](#), [3](#), [4](#), [5](#), [6](#), [7](#), [8](#), [11](#), [12](#), [13](#), [14](#)
- [47] Yin Zhou and Oncel Tuzel. Voxelnet: End-to-end learning for point cloud based 3d object detection. In *Proceedings of the IEEE conference on computer vision and pattern recognition*, pages 4490–4499, 2018. [1](#), [8](#)
- [48] Xizhou Zhu, Weijie Su, Lewei Lu, Bin Li, Xiaogang Wang, and Jifeng Dai. Deformable {detr}: Deformable transformers for end-to-end object detection. In *International Conference on Learning Representations*, 2021. [4](#)

A. Appendix

In this appendix, we provide additional details and results of the proposed method, Fast Point Transformer.

A.1. Experimental Details

In this section, we clarify the experimental settings for training models, latency evaluation, and model architectures in detail. Each experiment has been conducted with a fixed random seed for the reproducibility.

Training details. For 3D semantic segmentation, we use the same training configuration except the batch size for both ScanNet and S3DIS. We use the SGD optimizer with momentum and weight decay as 0.9 and 0.0001, respectively. The learning rate is scheduled by the linear warm-up and cosine annealing policy from the initial learning rate 0.1 to the final learning rate 0. We train models with batch size 16 for ScanNet and 8 for S3DIS with 80k iterations.

Latency evaluation. We describe the detailed setups that have been used during the inference time evaluation on Table 2 of the main paper. We measure the latency of each model with batch size 1 under the following environments:

1. CUDA version: 11.0
2. cuDNN version: 8.2.1
3. PyTorch version: 1.7.1
4. MinkowskiEngine version: 0.5.4
5. GPU: single NVIDIA Geforce RTX 3090
6. CPU: Intel(R) Core(TM) i7-5930K CPU @ 3.50GHz

Network architectures. Figure A1 illustrates detailed model designs of MinkowskiNet42 [5] and our Fast Point Transformer. To set the total parameter numbers to be similar, we adjust the feature dimensions as Hu et al. [13] does, resulting in similar parameter numbers; 37.9M for both models. For small models used in both Table 4 of the main paper and Table A2 of this supplement, we modify the number of residual blocks as the official code of MinkowskiNet [5] does. Table A1 provides the exact number of residual blocks.

A.2. Additional Experimental Results

In this section, we show further experimental results about the effect of model size on its performance, the proposed decomposition of positional encodings, and the class-wise IoU scores of both MinkowskiNet42[†] and our Fast Point Transformer on S3DIS [1] Area 5 test dataset.

mIoU vs. model size. Table A2 shows additional results with voxel size 2cm. Since Fast Point Transformer shows its robustness to the number of parameters with voxel size as 5cm and 10cm, Fast Point Transformer (smaller) still achieves 70.4% of mIoU score while MinkowskiNet

(smaller) only shows 68.0% with voxel size as 2cm. Interestingly, both MinkowskiNet and Fast Point Transformer show the largest performance drop with voxel size 2cm. We hypothesize that this is because the reduction of residual blocks reduces the receptive field of each model, and the reduced receptive field is not sufficient for the model to recognize a 3D scene with voxel size 2cm. **Decomposition of positional encodings.** We quantitatively measure how much memory the proposed decomposition of positional encodings can reduce. We measure the peak memory usage of both models with and without the decomposition as varying the local window size for neighbor points on ScanNet [6]. We keep the voxel size as 2cm for the all measurements. As shown in Table A3, the models with the proposed decomposition which has the space complexity of $\mathcal{O}(ND + KD)$ show an almost constant memory usage since the number of points N is much bigger than the number of neighbor points K . However, the models without the decomposition which has the space complexity of $\mathcal{O}(NKD)$ show a linearly growing usage of memory. Moreover, the model with local window size 7 raises the out-of-memory error in single NVIDIA Geforce RTX 3090 GPU whose VRAM capacity is 24GB. This results show the memory-efficient property of the proposed *lightweight* self-attention (LSA).

Detailed experimental results on S3DIS [1]. We report the class-wise IoU scores of both MinkowskiNet42[†] and the proposed Fast Point Transformer on S3DIS [1] Area 5 in Table A5. There is a large gap in the latency between point-based methods [16, 23, 34, 38, 45, 46] and voxel hashing-based methods [5] including out Fast Point Transformer as shown in Table A5. With 4.4 times faster speed than MinkowskiNet42[†] with rotation average, Fast Point Transformer outperforms MinkowskiNet42[†] with rotation average by 0.4 absolute percentage in mIoU.

A.3. Time Complexity Analysis

In this section, we analyze the time complexity of neighbor search used in both voxel hashing-based methods [5] including ours and point-based methods [34, 38, 45, 46]. We first recap the reported time complexity and wall time latency as shown in Table A4.

Table A1. **The number of residual blocks.** We apply the same configuration for both MinkowskiNet [5] and Fast Point Transformer. S_1, \dots, S_{16} denote the tensor stride in the feature map hierarchy.

Methods	Encoder				Decoder			
	S2	S4	S8	S16	S8	S4	S2	S1
baseline	2	3	4	6	2	2	2	2
small	2	2	2	2	2	2	2	2
smaller	1	1	1	1	1	1	1	1

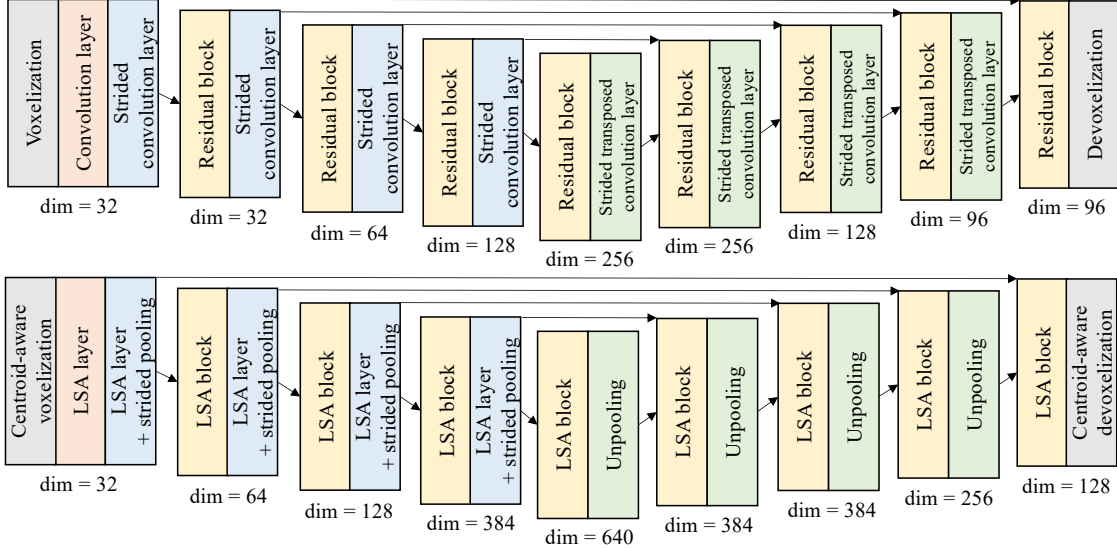


Figure A1. **Network architectures.** (Top) MinkowskiNet42 [5] and (Bottom) our Fast Point Transformer. LSA denotes the proposed lightweight self-attention. Note that both models have the same number of learnable parameters.

Table A2. **mIoU vs. model size.**

Methods	# Param. (M)		mIoU (%)	
		Rel. (%)		Δ
<i>Voxel size: 10cm</i>				
MinkowskiNet42 [†]	37.9	± 0.0	60.4	± 0.0
MinkowskiNet (small)	21.7	$\downarrow 42.7$	59.2	$\downarrow 0.8$
MinkowskiNet (smaller)	11.6	$\downarrow 69.4$	57.2	$\downarrow 3.2$
FastPointTransformer (ours)	37.9	± 0.0	65.3	± 0.0
FastPointTransformer (small)	20.2	$\downarrow 46.7$	65.7	$\uparrow 0.4$
FastPointTransformer (smaller)	10.8	$\downarrow 71.5$	65.6	$\uparrow 0.3$
<i>Voxel size: 5cm</i>				
MinkowskiNet42 [†]	37.9	± 0.0	66.6	± 0.0
MinkowskiNet (small)	21.7	$\downarrow 42.7$	65.9	$\downarrow 0.7$
MinkowskiNet (smaller)	11.6	$\downarrow 69.4$	63.9	$\downarrow 2.7$
FastPointTransformer (ours)	37.9	± 0.0	70.1	± 0.0
FastPointTransformer (small)	20.2	$\downarrow 46.7$	70.1	± 0.0
FastPointTransformer (smaller)	10.8	$\downarrow 71.5$	69.9	$\downarrow 0.2$
<i>Voxel size: 2cm</i>				
MinkowskiNet42 [†]	37.9	± 0.0	71.7	± 0.0
MinkowskiNet (small)	21.7	$\downarrow 42.7$	71.0	$\downarrow 0.7$
MinkowskiNet (smaller)	11.6	$\downarrow 69.4$	68.0	$\downarrow 3.7$
FastPointTransformer (ours)	37.9	± 0.0	72.0	± 0.0
FastPointTransformer (small)	20.2	$\downarrow 46.7$	71.3	$\downarrow 0.7$
FastPointTransformer (smaller)	10.8	$\downarrow 71.5$	70.4	$\downarrow 1.6$

MinkowskiNet [5] and Fast Point Transformer require

the same process for neighbor search since both methods benefit from voxel hashing. We analyze preparation and inference time complexity on Alg. 5 and Alg. 6, respectively. We denote ours as the representative method.

KPCConv [34] constructs a k -d tree before inference. With the official code of KPCConv, we analyze both preparation and inference time in Alg. 1 and Alg. 2, respectively.

PointWeb [45] uses a brute-force algorithm to search the k nearest neighbors. We analyze the time complexity of the brute-force algorithm in Alg. 3.

PACConv [38] and **Point Transformer** [46] do not require preparation steps for neighbor search. Thus we set the preparation time to constant time. For analyzing inference time, we have followed the official implementation. As both methods use the same algorithm for neighbor search, we denote PACConv as the representative method in Alg. 4.

Table A3. **Effect of the decomposition on memory usage.** k denotes the local window size which defines the maximum number of neighbor points, K .

k	Peak Memory Usage (GB)	
	with decomp. (ours)	without decomp.
3	3.613	9.519
5	3.892	23.245
7	4.494	Out of Memory

Algorithm 3 (PointWeb) Inference: $\mathcal{O}(MNK)$

Number of training points: N
Number of query points: M
Number of neighbors to search: K
for query = 1, 2, \dots , M **do**
 Best score buffer: $b[K]$
 for point = 1, 2, \dots , N **do**
 for $k = 1, 2, \dots, K$ **do**
 if $d(\text{query}, \text{point}) < b[k]$ **then**
 for $i = k - 1, \dots, k + 1$ **do**
 $b[i] = b[i - 1]$
 end for
 end if
 $b[k] = d(\text{query}, \text{point})$
 end if
 end for
 end for
end for

Algorithm 4 (PAConv) Inference: $\mathcal{O}(MN \log K)$

Number of training points: N
Number of query points: M
Number of neighbors to search: K
for query = 1, 2, \dots , M **do**
 $H = \text{InitHeap}()$ $// \mathcal{O}(K)$
 $\text{MinD} = 10^{10}$
 $\text{MinIdx} = 0$
 for point = 1, 2, \dots , N **do**
 if $d(\text{point}, \text{query}) < \text{MinD}$ **then**
 $\text{Reheap}(H, \text{MinD}, \text{MinIdx}, K)$ $// \mathcal{O}(\log K)$
 $\text{MinD} = d(\text{point}, \text{query})$
 $\text{MinIdx} = \text{point}$
 end if
 end for
 $\text{Heapsort}(H, \text{MinIdx}, \text{MinD}, K)$ $// \mathcal{O}(K \log K)$
end for

Algorithm 5 (Ours) Hash Table Construction: $\mathcal{O}(N)$

Number of training points: N
An empty hash table: h
for point = 1, 2, \dots , N **do**
 $\text{Insert}(h, \text{point})$ $// \mathcal{O}(1)$
end for

Algorithm 6 (Ours) Inference: $\mathcal{O}(M)$

Number of query points: M
A constructed hash table: \bar{h}
for query = 1, 2, \dots , M **do**
 $\text{Lookup}(\bar{h}, \text{query})$ $// \mathcal{O}(1)$
end for

Table A4. **Time complexity analysis.**

Methods	Neighbor Search	
	Preparation	Inference
PointNet [23]	\times	\times
SPGraph [16]	\times	\times
PointWeb [45]	$\mathcal{O}(1)$	$\mathcal{O}(MNK)$
KPConv <i>deform</i> [34]	$\mathcal{O}(N \log N)$	$\mathcal{O}(KM \log N)$
PAConv [38]	$\mathcal{O}(1)$	$\mathcal{O}(MN \log K)$
PointTransformer [46]	$\mathcal{O}(1)$	$\mathcal{O}(MN \log K)$
MinkowskiNet [5]	$\mathcal{O}(N)$	$\mathcal{O}(M)$
FastPointTransformer (ours)	$\mathcal{O}(N)$	$\mathcal{O}(M)$

Algorithm 1 (KPConv) Tree Construction: $\mathcal{O}(N \log N)$

Number of training points: N
An empty tree: T
for point = 1, 2, \dots , N **do**
 $\text{Insert}(T, \text{point})$ $// \mathcal{O}(\log N)$
end for

Algorithm 2 (KPConv) Inference: $\mathcal{O}(KM \log N)$

Number of training points: N
Number of query points: M
Number of neighbors to search: K
Constructed k -d tree: \bar{T}
 k -th nearest neighbors dictionary: $S = \{\}$
for query = 1, 2, \dots , M **do**
 $\text{arr} = []$
 for $i = 1, 2, \dots, K$ **do**
 $\text{point} = \text{SearchClosest}(\bar{T}, \text{query})$ $// \mathcal{O}(\log N)$
 $\bar{T} = \text{Pop}(\bar{T}, \text{point})$ $// \mathcal{O}(\log N)$
 $\text{arr.append}(\text{point})$
 end for
 $S[\text{query}] = \text{arr}$
end for

A.4. Qualitative Results

In this section, we show further qualitative results of consistency scores, 3D semantic segmentation results, and 3D object detection on ScanNet [6]. Figure A2 shows the point-wise consistency scores of MinkowskiNet42[†] and our Fast Point Transformer. As shown in Figure A2, Fast Point Transformer outputs more consistent predictions than MinkowskiNet42[†]. In addition to this consistency, Fast Point Transformer predicts more accurate 3D semantic labels (Figure A3) and 3D bounding boxes (Figure A4) qualitatively.

Table A5. **Detailed experimental results on S3DIS [1] Area 5 test dataset.** Note that the latency of each method denotes the per-scene wall-time latency normalized by that of Fast Point Transformer. Numbers except the latency means percentage values (%).

Methods	Latency	mIoU	mAcc	ceil.	floor	wall	beam	col.	wind.	door	table	chair	sofa	book.	board	clut.
PointNet [23]	136.5	41.1	49.0	88.8	97.3	69.8	0.1	3.9	46.3	10.8	59.0	52.6	5.9	40.3	26.4	33.2
SPGraph [16]	137.4	58.0	66.5	89.4	96.9	78.1	0.0	42.8	48.9	61.6	84.7	75.4	69.8	52.6	2.1	52.2
PointWeb [45]	87.4	60.3	66.6	92.0	98.5	79.4	0.0	21.1	59.7	34.8	76.3	88.3	46.9	69.3	64.9	52.5
KPConv <i>deform</i> [34]	760.5	67.1	72.8	92.8	97.3	82.4	0.0	23.9	58.0	69.0	81.5	91.0	75.4	75.3	66.7	58.9
PAConv [38]	211.5	66.6	73.0	94.6	98.6	82.4	0.0	26.4	58.0	60.0	80.4	89.7	69.8	74.3	73.5	57.7
PointTransformer [46]	135.9	70.4	76.5	94.0	98.5	86.3	0.0	38.0	63.4	74.3	89.1	82.4	74.3	80.2	76.0	59.3
MinkowskiNet42 [†]	0.5	66.0	73.3	93.2	97.0	84.0	0.0	25.7	63.9	66.4	76.9	88.9	58.4	70.1	78.0	54.9
+ rotation average	4.4	67.1	73.5	93.9	97.1	85.2	0.1	28.3	64.5	70.3	76.8	90.0	57.2	70.9	81.1	56.7
FastPointTransformer	1.0	67.5	74.7	91.5	97.4	86.0	0.2	40.4	60.8	66.7	79.6	87.7	58.6	73.7	77.2	57.3
+ rotation average	8.1	68.5	75.5	90.0	96.0	86.2	0.0	47.1	61.3	69.7	81.1	88.2	60.9	74.2	78.2	57.3

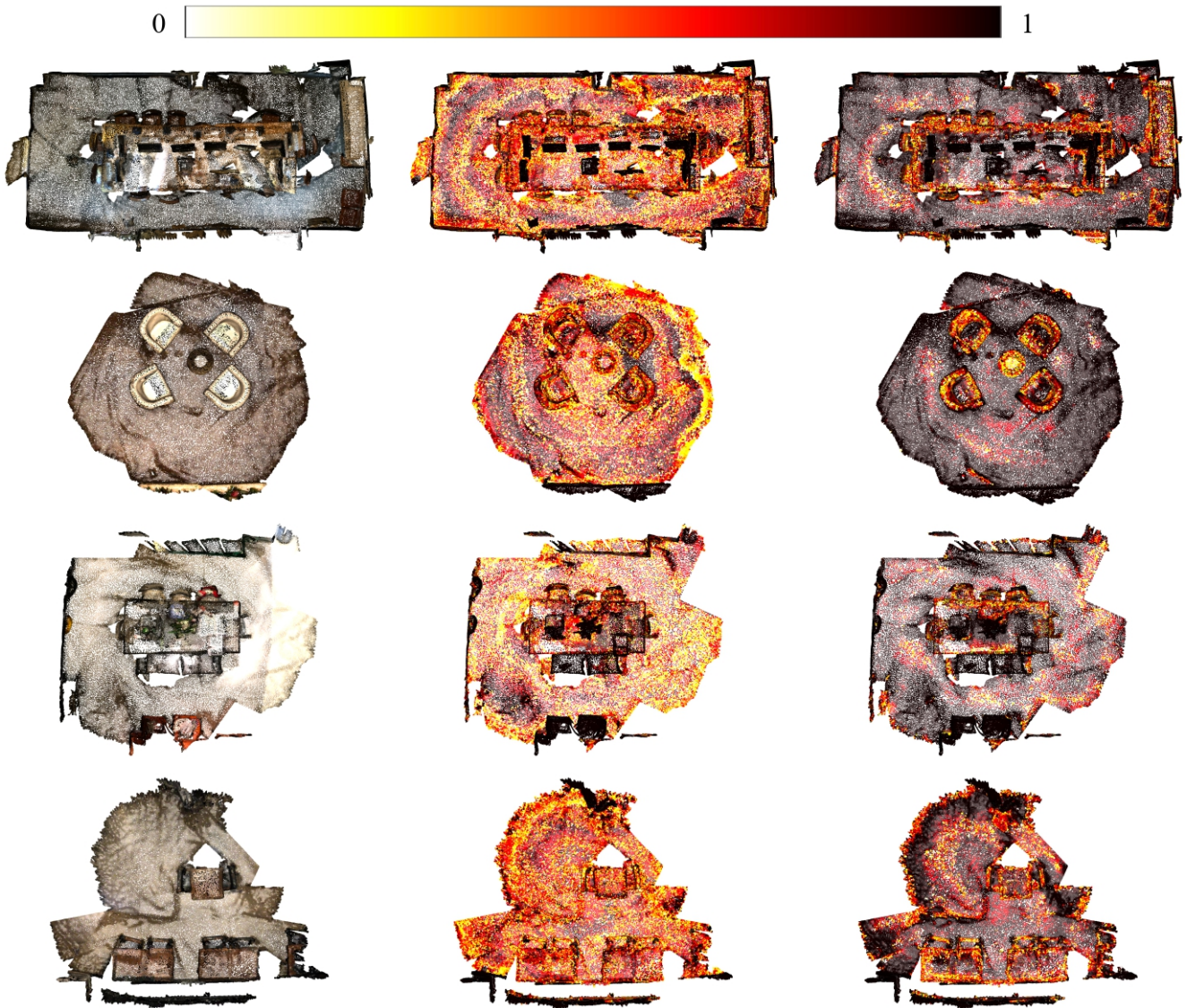


Figure A2. **Qualitative results of consistency scores (CScore) on ScanNet [5].** (Left) Input point cloud, (Middle) CScore of MinkowskiNet42[†], and (Right) CScore of the proposed Fast Point Transformer. Both models are trained with voxel size as 10cm.

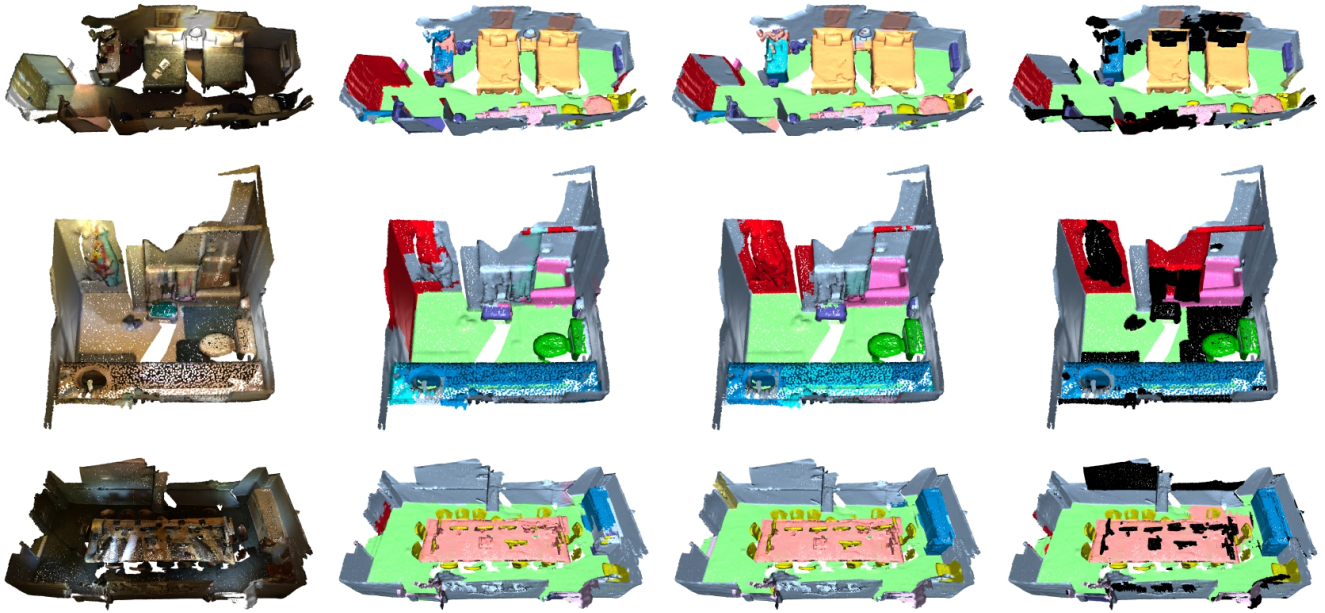


Figure A3. **Qualitative results of 3D semantic segmentation on ScanNet [5].** (First column) Input point cloud, (Second column) Predicted semantic labels by MinkowskiNet42[†], (Third column) Predicted semantic labels by the proposed Fast Point Transformer, and (Fourth column) Ground truth. Both models are trained with voxel size as 10cm.

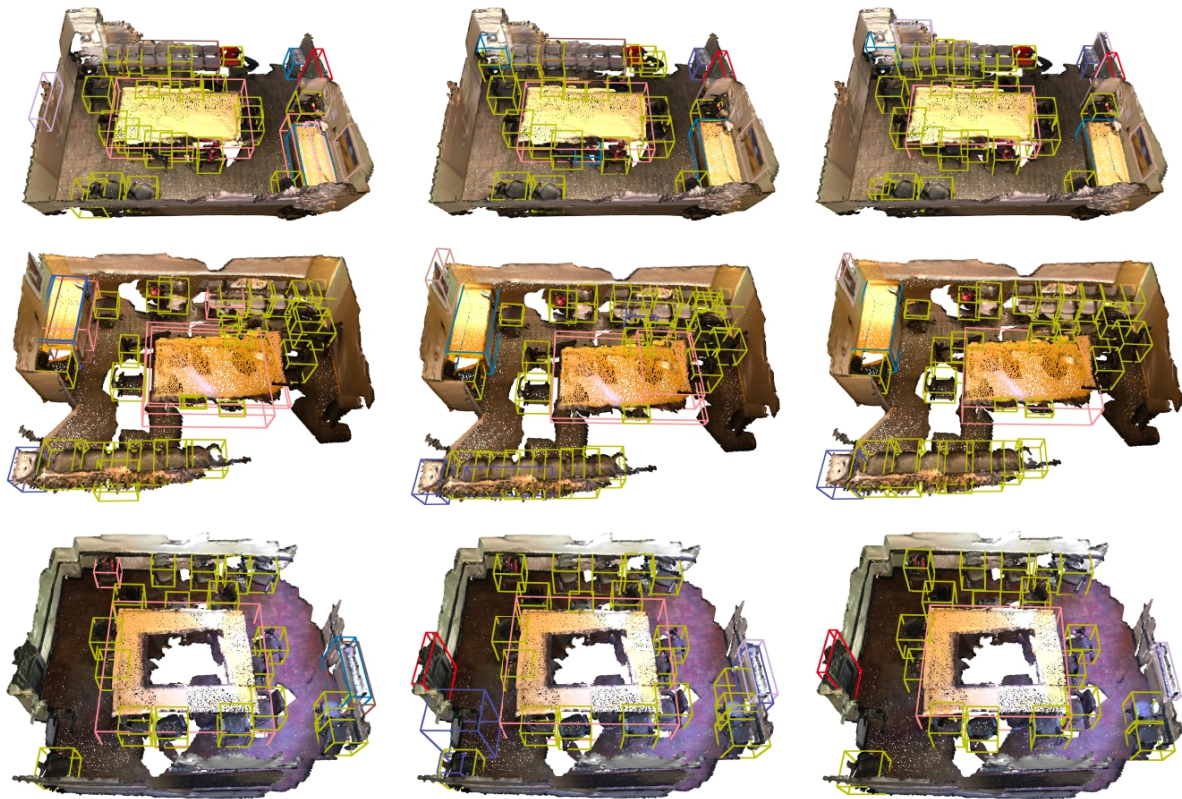


Figure A4. **Qualitative results of 3D object detection on ScanNet [5].** (Left) Predicted bounding boxes by VoteNet [22] with MinkowskiNet backbone, (Middle) Predicted bounding boxes by VoteNet [22] with the proposed Fast Point Transformer backbone, and (Right) Ground truth.

A.5. Notations

$\mathcal{P}^{\text{in}} = \{(\mathbf{p}_n, \mathbf{i}_n)\}$	Input point cloud
$\mathbf{p}_n \in \mathbb{R}^3$	The n -th point coordinate
$\mathbf{i}_n \in \mathbb{R}^{D_{\text{in}}}$	The n -th input point feature
$\mathcal{P}^{\text{out}} = \{(\mathbf{p}_n, \mathbf{o}_n)\}$	Output point cloud
$\mathbf{o}_n \in \mathbb{R}^{D_{\text{out}}}$	The n -th point feature
$\mathcal{V} = \{(\mathbf{v}_i, \mathbf{f}_i, \mathbf{c}_i)\}$	Input voxels with centroids
$\mathbf{v}_i \in \mathbb{R}^3$	The i -th voxel center coordinate
$\mathbf{f}_i \in \mathbb{R}^{D_{\text{in}}}$	The i -th input voxel feature
$\mathbf{c}_i \in \mathbb{R}^3$	The i -th voxel centroid coordinate
$\mathcal{M}(i)$	A set of point indices within the i -th voxel
Ω	A permutation-invariant operator (<i>e.g.</i> , average)
$\mathcal{V}' = \{(\mathbf{v}_i, \mathbf{f}'_i, \mathbf{c}_i)\}$	Output voxels with centroids
$\mathbf{f}'_i \in \mathbb{R}^{D_{\text{out}}}$	The i -th output voxel feature
$\mathcal{N}(i)$	A set of neighbor voxel indices the i -th voxel
\mathbf{e}_n	The centroid-to-point positional encoding
δ_{enc}	An encoding layer used in centroid-to-point positional encoding
\mathbf{o}_n	The n -th output point feature of the output point cloud \mathcal{P}^{out}
\oplus	A vector concatenation operation
$a(\cdot)$	An attention operation
ψ	A value projection layer in attention operations
\mathbf{g}_i	A centroid-aware voxel feature
δ_{rel}	A discretized positional encoding layer
δ_{abs}	A continuous positional encoding layer